Small-Angle Neutron Scattering from Diffuse Interfaces. 2. Polydisperse Shells in Water−*n*-Alkane−$C_{10}E_4$ Microemulsions

M. Gradzielski and D. Langevin

Laboratoire de Physique Statistique, Ecole Normale Superieure, 24 rue Lhomond, F-75231 Paris cedex 05, France

L. Magid

Department of Chemistry, University of Tennessee, Knoxville, Tennessee 37996-1600

R. Strey*

Max-Planck-Institut für Biophysikalische Chemie, Postfach 2841, D-37018 Göttingen, Germany

Received: March 17, 1995; In Final Form: June 27, 1995[⊗]

A new model for the shell structure of surfactants in droplet microemulsions is described in which the scattering length density distribution of the interface is treated as a Gaussian profile. The corresponding particle form factor and scattering intensity on an absolute scale are derived in analytical form for the case of both monodisperse and polydisperse droplets. It is compared with the more conventional model of concentric shells with sharp boundaries. We find that both models differ mainly in their high-q behavior. We use both models to describe experimental SANS spectra of droplet microemulsions in shell contrast. The new model proves to provide a more accurate description of the experimental data.

I. Introduction

Microemulsions are microstructured mixtures of water, oil, and surfactant. Here two immiscible liquids, water and oil, form a single phase, stabilized by the presence of the surfactant molecules. Microemulsions are typically of low viscosity, transparent, optically isotropic, and thermodynamically stable, a feature distinguishing them from conventional emulsions.[1,2] The structural buildup of microemulsions has been the subject of numerous experimental and theoretical investigations. Despite the fact that they have been known for more than 50 years,[3−5] their detailed microstructure and the principles that govern it are still not fully understood. Generally three principal structural types of microemulsions have been distinguished:

(i) Droplets of oil covered by a surfactant film in a continuous aqueous medium (O/W microemulsion).[6,7]

(ii) Droplets of water covered by a surfactant film in a continuous oily medium (W/O microemulsion).[8−11]

(iii) Bicontinuous microemulsion, i.e., both hydrophobic and hydrophilic parts of the microemulsion are continuous.[12−16]

The structure of a given microemulsion system will depend on the relative amounts of oil and water present and, of course, on the particular choice of surfactant or surfactant plus cosurfactant. In particular, the nature of the amphiphile is the major determinant of the natural curvature the amphiphilic film tries to adopt and also of the total internal interface in the system. This natural or spontaneous curvature in turn depends sensitively on parameters such as temperature which therefore have a profound influence on the structure that is attained by a given surfactant system.[17]

For investigations of the microstructure of microemulsions scattering methods are in general a suitable tool and have frequently been used to study the different structures.[8,13,18−22,31,43,54] Particularly suited for microemulsion systems are small-angle neutron scattering (SANS) experiments. With momentum transfers q ($=4\pi \sin(\theta/2)/\lambda$) of 0.006−0.6 Å^{-1} the typical microemulsion dimensions of 10−1000 Å can be examined. In addition, in SANS experiments one can easily change the contrast conditions by using correspondingly deuterated water or oil, without significantly changing the phase behavior and domain sizes of the microemulsions.[23−26] The most profound effect of deuteration on the phase behavior is the isotopic substitution of water since D_2O exhibits stronger hydrogen bonding than H_2O.[27] However, even this effect is usually small and can be compensated for by minor temperature changes in the non-ionic systems studied here.

From a change in the contrast conditions, more information is accessible, and a more refined picture of the particles can be obtained.[23] A particular contrast condition that yields very valuable information is the "shell contrast", where deuterated water and oil are used together with hydrogenated surfactant. By doing so, the scattering length densities of oil and water are almost exactly matched and the scattering will almost exclusively be due to the coherent scattering of the surfactant film. For the case of microemulsion (O/W or W/O) droplets one will observe only the scattering from a shell. Moreover, the scattering function of a shell yields more precise information, especially regarding the polydispersity of the corresponding system, if compared with the scattering of an equivalent solid sphere.[28−31]

II. Scattering Theory. Model of the Microemulsion Droplet

Microemulsion droplets in shell contrast are often described by a model of sharp boundaries, i.e., a model of concentric shells. This model is certainly well suited for describing the scattering curves of solid particles, such as dispersions of alkaline-earth carbonates or silica particles, stabilized by a hydrophobic layer in a hydrophobic medium.[32−34] It has also frequently been used to describe micellar systems, especially

* To whom correspondence should be addressed.

[⊗] Abstract published in *Advance ACS Abstracts,* August 1, 1995.

0022-3654/95/2099-13232$09.00/0

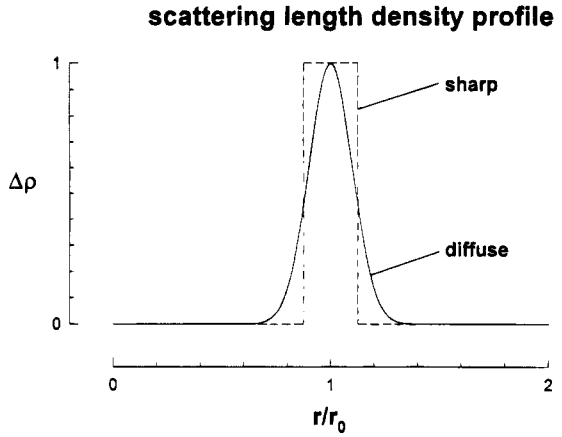

Figure 1. Schematic variation of the scattering length density in the microemulsion droplet: with sharp boundaries (dashed line); with a Gaussian distribution of the scattering length density (full line).

in order to distinguish between the hydrophobic core and the region of the polar head groups.[35-39] In addition it has been employed successfully to analyze scattering data from vesicular systems,[40,41] where the interior and the exterior of the vesicles generally will have exactly identical scattering length densities.

However, this model does not take into account the interpenetration of the solvents. On one side of the layer, the oil penetrates into the hydrophobic part of the surfactant, and on the other side water hydrates the hydrophilic part of the surfactant. This effect should be particularly pronounced for non-ionic surfactants of the type C_iE_j (*n*-alkylpoly(glycol ethers)), since the head groups are short poly(ethylene oxides), which are very well soluble in water, so that the head group of the surfactant will be strongly hydrated and extend well into the surrounding aqueous medium.

Therefore a more realistic description of such systems should be a model that takes into account the diffuseness of the amphiphilic film. A simple way of describing the density profile of the film is assuming a Gaussian distribution of the scattering length density $\varrho(r)$. A similar Gaussian profile for the scattering density of the interface has been employed before for describing the scattering patterns of bicontinuous microemulsions and L_3 phases which possess a locally flat interface.[42]

A. Diffuse Interfaces. Here we want to consider the case of spherical symmetry. The q dependence of the scattered intensity of spherical droplets in film contrast is derived assuming the droplets to be surrounded by a diffuse film. In this case the contrast varies through the film as shown schematically in Figure 1. For simplicity the contrast is assumed to be described by a Gaussian profile. For this shell contrast condition, the scattering length density may then be characterized by two parameters, i.e., the maximum contrast $\Delta\varrho$ and the thickness parameter t of the Gaussian function

$$\varrho(r) = \Delta\varrho \exp(-(r-r_0)^2/2t^2) \quad (1)$$

where the maximum difference $\Delta\varrho$ between the matched bulk scattering lengths and the film is reached at the center of the film, at $r = r_0$. Furthermore the total contrast has to fulfill the condition

$$\Delta\varrho\frac{4\pi}{3}(r_1^3 - r_2^3) = \Delta\varrho\frac{4\pi}{3}\left(3\delta r_0^2 - \frac{\delta^3}{4}\right) = \Delta\varrho 4\pi\int_0^{+\infty} r^2\varrho(r)\,dr \quad (2)$$

with

$$\int_{-\infty}^{+\infty} r^2\varrho(r)\,dr = (2\pi)^{1/2}t(r_0^2 + t^2) \quad (3)$$

Then

$$t = \frac{\delta}{\sqrt{2\pi}}\frac{r_0^2 + \delta^2/12}{r_0^2 + t^2} \approx \frac{\delta}{\sqrt{2\pi}} \quad (4)$$

where δ is the thickness of the shell model with sharp boundaries at r_1 and r_2 with an equivalent total scattering intensity, and $r_0 = (r_1 + r_2)/2$. The approximation in eq 4 holds for $r_0 \gg t$, and it is the exact result for the planar case.[42] One might note that the error of this approximation remains less than 2% even for $\delta/r_0 = 0.5$, that is, it should hold well for most realistic cases.

The form factor of such a density distribution, i.e., the angle-dependent intensity function that arises because of intraparticle interferences, is then directly related to the Fourier transform of the corresponding distribution of the scattering length density. For the case of radially symmetrical particles, this Fourier transform is simply given by a one-dimensional Fourier integral:

$$F(q) = -4\pi\int_0^{+\infty} r^2\varrho(r)\frac{\sin(qr)}{qr}\,dr \quad (5)$$

By inserting eq 1 into eq 5, one has the Fourier integral of a Gaussian function, which can readily be calculated (if one allows the lower boundary of the integral to go to $-\infty$, which is valid if the thickness parameter t is much smaller than the mean radius r_0) and yields an analytical expression for the form factor $F(q)$ of the particle considered:

$$F(q) = -4\pi\Delta\varrho\frac{\delta}{q}\exp(-q^2t^2/2)(r_0 \sin qr_0 + qt^2 \cos qr_0) \quad (6)$$

Finally the particle form factor $P(q)$ is in general given by

$$P(q) = F(q)^2 \quad (7)$$

so that

$$P(q) = 16\pi^2(\Delta\varrho)^2(\delta^2/q^2)\exp(-q^2t^2)(r_0 \sin qr_0 + qt^2 \cos qr_0)^2 \quad (8)$$

which is the result for monodisperse shell-structured particles. Obviously for the monodisperse case we still expect the minima of the form factor to go to zero scattering intensity.

In a next step we may consider a more realistic system with some degree of polydispersity. This polydispersity may be described by a Gaussian distribution function of the mean radii of the shell structured particles. Such a Gaussian function has been employed successfully before to describe the size distribution in microemulsion systems[43] or vesicular systems.[40]

The form factor of such a system can be evaluated by summing, or respectively integrating, over all individual form factors weighted by this distribution function. Again this integral can be solved analytically if one allows the lower boundary of the integral to go to $-\infty$, which is justified as long as the width of the distribution function σ is significantly smaller than the mean radius r_0. This condition is still well fulfilled for $\sigma/r_0 < 0.35$. As we verified, in this range the numerical integration within the proper limits and the analytical approximation still yield practically indistinguishable results. After taking into account all the terms that arise in the integration over a Gaussian (see the Appendix for details), we obtain the form factor of a shell-structured system, where this shell itself has a Gaussian density profile, and where the mean radii of an

ensemble of these shells have a Gaussian distribution around a mean value r_0:

$$P(q) = 16\pi^2(\Delta\varrho)^2(\delta^2/q^2)\exp(-q^2t^2)(t_1(q) + t_2(q) + t_3(q) + t_4(q)) \quad (9)$$

with

$$t_1(q) = {}^1/_2q^2t^4(1 + \cos 2qr_0e^{-2\sigma^2q^2}) \quad (9a)$$

$$t_2(q) = qt^2(r_0 \sin 2qr_0 + 2q\sigma^2 \cos 2qr_0)e^{-2\sigma^2q^2} \quad (9b)$$

$$t_3(q) = {}^1/_2r_0{}^2(1 - \cos 2qr_0e^{-2\sigma^2q^2}) \quad (9c)$$

$$t_4(q) = {}^1/_2\sigma^2(1 + 4qr_0 \sin 2qr_0e^{-2\sigma^2q^2} + \cos 2qr_0(4\sigma^2q^2 - 1)e^{-2\sigma^2q^2}) \quad (9d)$$

One advantage of the outlined approach is that it yields an analytical expression for the particle form factor that can conveniently be employed for calculation of absolute intensities. Despite being a realistic model incorporating both the diffuseness of the particle shell as well as the size polydispersity, one still finds a relatively simple expression for the scattering of such systems. Moreover the considered model with its diffuse boundaries should be a realistic description of the situation in typical microemulsions, especially those formed by non-ionic surfactants of type C_iE_j and it will be compared with actual data in section III.

The experimentally observed scattering intensity, i.e., the coherent part of the differential cross section, is then given by

$$I(q) = NP(q)\,S(q) \quad (10)$$

where N is the number density of the aggregates and $S(q)$ the interparticle structure factor.

The prefactor of eq 9 relating the scattering intensity to absolute units may now be expressed in terms of the volume v_s and a specific surface area a_s of the surfactant molecule at the mean radius r_0 of the corresponding shell. If we also express the number density in terms of v_s, a_s, r_0, and σ we finally obtain

$$I(q) = \frac{4\pi\phi_s}{1 + \sigma^2/r_0{}^2}\frac{v_s(\Delta\varrho)^2}{a_sr_0{}^2q^2}e^{-q^2t^2}(t_1(q) + t_2(q) + t_3(q) + t_4(q))S(q) \quad (11)$$

for the scattered intensity.

Of course, we have $S(q) = 1$ for the dilute limit. For the moderately concentrated samples studied, a suitable $S(q)$ function can be inserted into eq 11 which still for larger q will become unity.

One observes that the mean radius r_0 is easily found from the characteristic dip in the scattering pattern being a remnant of the first minimum of the Bessel function involved. The mean radius can therefore be used as a rather accurate measure for the mean curvature $\langle H\rangle = 1/r_0$, which is a characteristic quantity for a microemulsion.[30]

B. Step Profiles. The conventional treatment of a series of concentric shells ($i = 1, 2, \ldots$) arises as one inserts a constant (or a series of constants) for r_i in eq 5. As mentioned above, this model has already found ample application for the interpretation of scattering data. We use here a single shell model for which the scattering amplitude is given by

$$P(q) = F(q)^2 = \Delta\varrho^2[V_2\phi(qr_2) - V_1\phi(qr_1)]^2 \quad (12)$$

with $V_i = (4\pi/3)r^3{}_i$ and $\phi(x) = 3(\sin x - x\cos x)/x^3$. Equation 12 is valid for the monodisperse case, and again the polydisperse scattering intensity can be calculated by integrating over the respective $f(r)$:

$$I(q) = NS(q)\int_0^\infty f(r)\,P(q,r)\,dr \quad (13)$$

It might be mentioned that in some cases, such as that of a Schulz distribution of radii,[44] there are analytic solutions for the particle form factor. However, we used here for convenience a numerical integration over a Gaussian distribution:

$$f(r) = (2\pi\sigma^2)^{-1/2}\exp(-(r - r_0)^2/2\sigma^2) \quad (14)$$

in order to have the same distribution function for the comparison of our new model with the conventional model of sharp interfaces. Therefore, the outcome of this comparison should depend not on the choice of the distribution function but exclusively on the scattering properties of the interfacial film.

C. Numerical Calculations. In the following we want to compare our new model for the diffuse interface with that of a step profile for the scattering length density. At first, we might note here that the form factor for the monodisperse case (eq 8) will still go to zero at

$$qr_0 = \arctan(qt^2/r_0) + n\pi \quad (15)$$

as does that of the model with sharp boundaries (or in general any model with concentric shells of spherical symmetry). Therefore, the nonzero scattering intensity at the minima of the scattering curve does not depend on the choice of the particular structural buildup of the particles but is an effect entirely due to their polydispersity and, of course, to the finite resolution of the scattering experiment. Especially in SANS experiments, one has a relatively large wavelength spread, collimation effects, and the spatial resolution of the detector elements.

We may now proceed to compare our new model with the more conventional one of concentric shells with sharp boundaries. It might be pointed out here that both models are characterized by the same number of parameters. In Figure 2 form factors for thin shells (the thickness is a tenth of the mean radius r_0 for the model with sharp boundaries; for the model with the Gaussian profile the thickness parameter t was chosen in such a way as to yield the same total mass of the shell, i.e., an identical total scattering intensity) have been calculated for polydisperse systems, where the standard deviation σ of the Gaussian distribution describing the polydispersity was chosen to be 10 and 20%, respectively, of the mean radius r_0.

One readily observes that both models yield a very similar scattering pattern in the low-q range, i.e., for $qr_0 < 5$, which is mainly determined by the radius and the polydispersity of the respective particles. An evaluation of the parameters mean radius and polydispersity (where the effect of the polydispersity is to smear out the minima in the scattering curve which would go to zero for a monodisperse system) from experimental data therefore should yield very similar values for both models. However, both differ with respect to their behavior in the high-q range (the Porod region). Here the curves with the Gaussian density profile show a much faster decay than the form factor for shells with sharp boundaries. Such a behavior is generally to be expected for a system that has a more diffuse boundary of the scattering length density,[42,45,55] whereas for shelllike particles with a thin shell a q^{-2} dependence should be observed.

The decay in the high-q range depends markedly on the choice of the thickness parameter t, a fact that is illustrated in

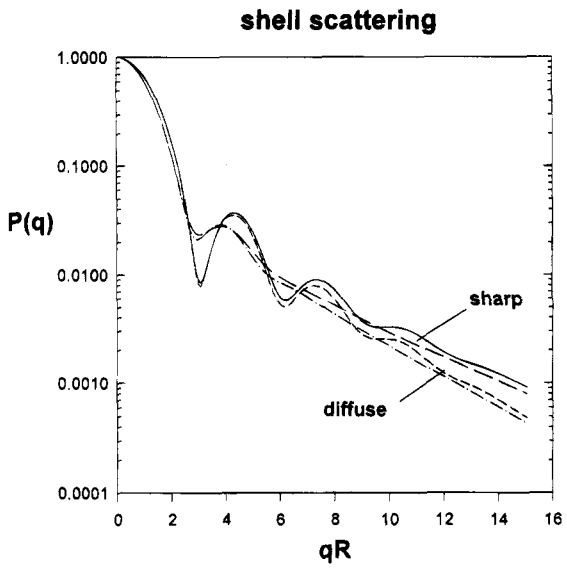

Figure 2. Calculated form factors $P(q)$ of shell structured particles with the polydispersity given by a Gaussian distribution of the radii. Model of concentric spherical shells with sharp boundaries: Full line: $\delta = 0.1r_0$, $\sigma = 0.1r_0$; long dash: $\delta = 0.1r_0$, $\sigma = 0.2r_0$. The model with diffuse boundaries as suggested in this paper: Short dash: $t = 0.08r_0$, $\sigma = 0.1r_0$; Dash−dotted: $t = 0.08r_0$, $\sigma = 0.2r_0$.

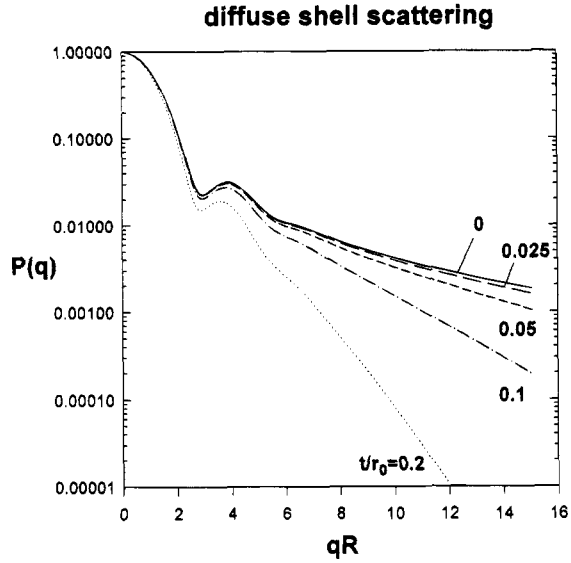

Figure 3. Calculated form factors $P(q)$ as given by eq 9 for various choices of the thickness parameter t: In all cases the polydispersity parameter was $\sigma = 0.2r_0$. Note the striking decay for increasing t.

Figure 3, which gives the calculated form factors for various choices of t. Of course, in the limit $t \to 0$ we regain the q^{-2} behavior of shells with sharp boundaries, whereas the decay of the intensity will be increasingly faster for larger t. This means that the thickness parameter t of our model is very sensitively reflected in the high-q pattern of the scattering curves. The choice of the thickness parameter t has only a small effect on the scattering curve in the low-q range. However, the thickness of the film will significantly influence the absolute scale of the scattering intensity. The thickness δ of the film (and through eq 4 also t) are related to v_s/a_s. Therefore the intensity is directly proportional to δ or $1/a_s$ for constant v_s at a given concentration. Therefore, one should be able to determine a_s precisely from an accurate analysis of the absolute scattering intensities.

In summary we may state that the applicability of both models should mainly be judged from the asymptotic behavior of the scattering intensity in the high-q range, where both models yield

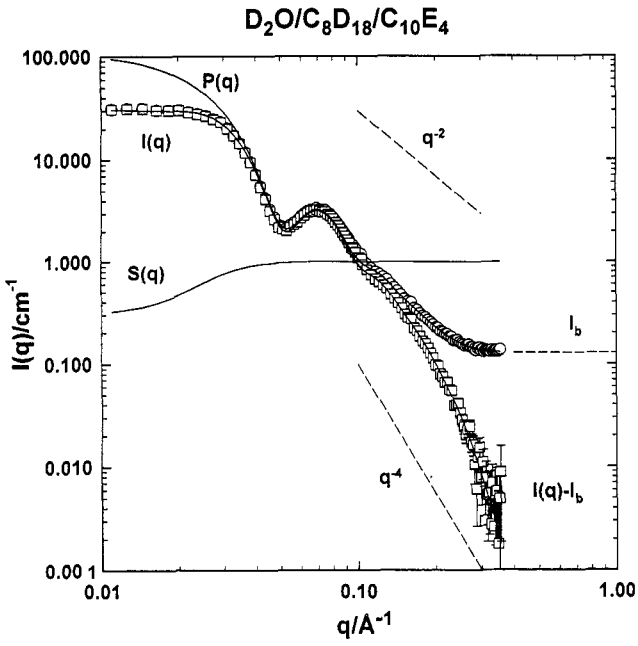

Figure 4. SANS intensity curves for an O/W microemulsion of the $D_2O/C_8D_{18}/C_{10}E_4$ system at a droplet volume fraction of $\phi = 0.148$ at $T = 8.7$ °C. The microemulsion was located at the phase boundary in equilibrium with the excess oil phase. The solid line is the fit according to eq 11 using the empirical structure factor $S(q)$ (which is a dimensionless quantity) also shown. Note that extending the measurement of the scattering curve to large enough q allows a precise determination of the background scattering I_b. Subtraction of I_b from the scattering curve reveals the exponentially steep decay until the statistical error becomes large, as can be estimated from the scatter at high q. For most of the curve the error bars are well within the symbol width and hence not visible.

significantly different predictions. For obtaining values for the mean radii of the particles and their polydispersity, both models yield similar results since the detailed structure of this shell is mainly reflected in the high-q range. This may easily be understood if we recall that structural information on small length scales should increasingly be reflected in the high-q range, i.e., the higher q, the more refined the spatial resolution.

III. Comparison with Experimental Data

In this section we demonstrate the applicability of our model for the description of experimental data from SANS on droplet microemulsion systems. The particular systems examined consist of three components: water, oil, and a non-ionic surfactant, i.e., the simplest possible composition of a microemulsion providing the most transparent experimental conditions. The nonionic surfactant is of the type C_iE_j. The advantage of choosing this surfactant type is that it has been shown in extensive studies that the natural curvature in these systems can finely be adjusted by changing the temperature.[30,46-48] By increasing the temperature, one reduces continuously the natural curvature until finally negative values are achieved, i.e., the microemulsion will form normal structures at low temperature, prefer a zero curvature at the phase inversion temperature, and at still higher temperatures reversed structures form. This structural sequence has been verified by means of freeze fracture electron microscopy,[30] NMR self-diffusion,[49] and small angle scattering experiments.[50] A more detailed description is given elsewhere.[30]

In Figure 4 a SANS scattering curve is presented for the $D_2O/C_8D_{18}/C_{10}E_4$ system, i.e., in the shell contrast, since the scattering length densities of deuterated water and deuterated n-octane are almost equal. The choice of this surfactant seems to be

particularly suited for our model, because here the hydrophilic and hydrophobic parts are of about the same size. Assuming a similar degree of penetration for both sides of the film, the density profile will be nearly symmetric. The experiment was performed at 8.7 °C where a macroscopic oil-rich phase is in equilibrium with the O/W microemulsion droplets. The data were taken on D17 at the ILL in Grenoble (λ = 5 Å, $\Delta\lambda/\lambda$ = 0.1, data treatment as in ref 42).

Several features are immediately seen. First, there is the fingerprint of the Bessel function at intermediate q. Second, the measurements are extended to sufficiently high q to be able to determine the background scattering intensity I_b. Third, subtracting the background intensity reveals the exponentially steep decay. Fourth, there is a systematic deviation at low q from the prediction of the particle form factor for ideal noninteracting spheres.

The experimental scattering curves were fitted with the model given by eq 11. A good agreement between the experimental data and the model (solid lines), as previously for a different system,[30,51] is observed. The individual fit parameters are sensitive to different regions of the scattering curve. In particular, we obtained r_0 = 56.0 Å from the position of the minimum, σ = 10.2 Å from the smearing of the minimum/maximum region, t = 5.8 Å from the large-q decay, and a_s = 60 Å^2 from the absolute scale. The background I_b = 0.128 cm^{-1} was found from the largest q measured. For the remaining parameters in eq 11 we used the known values for v_s = 579 Å^2, $\Delta\varrho = 6.11 \times 10^{10}$ cm^{-2}, and ϕ_s = 0.0741. Calculating δ using eq 4, we find δ = 14.8 Å which is close to the 13.8 Å found by Lee and Chen for the same system but for the bicontinuous region.[55]

A comparison the model of sharp boundaries will be performed below. This model yields also a good description of the experimental data in the immediate-q part. However, only the model with diffuse boundaries can describe the exponentially fast decay in the high-q range, where the model with sharp boundaries approaches only a q^{-4} decay (as discussed in section II). Accordingly, the diffuse boundary model is in better agreement with the experimental data. In addition, it also yields an almost perfect description around the minimum/maximum regime, from which a fairly small polydispersity of the investigated samples is visible. Note that the smearing of the data due to the finite resolution and wavelength spread is still included in the experimental spectra.

At low q the repulsive interaction between the droplets leads to a decreased intensity, as demonstrated by the empirical structure function $S(q)$ shown in Figure 4. Here we refrain from further investigated the nature of the repulsive interaction. We note only that the soft nature of the droplets is clearly evidenced by the existence of the shape fluctuations of the droplets in neutron spin−echo experiments (NSE). Therefore, using a hard-sphere structure factor may be a too simplified view.

However, reducing the volume fraction of the droplets $S(q)$ can be made unity for all q, irrespective of the particular interaction. Such experiments are shown in Figure 5. The SANS curves here were obtained for the $D_2O/C_{10}D_{22}/C_{10}E_4$ system at 10 °C. Again the microemulsion droplets were in equilibrium with the excess oil phase. The volume fraction of the droplets was 0.01 and 0.03, respectively, which ensures that at this low volume fractions the particle form factor should almost exclusively determine the scattering curve. Interparticle interferences should not be significant, i.e., the structure factor should be negligible, since the microemulsion aggregates of this uncharged system interact only via their steric repulsion, and this effect should be small for volume fractions less than 0.1.

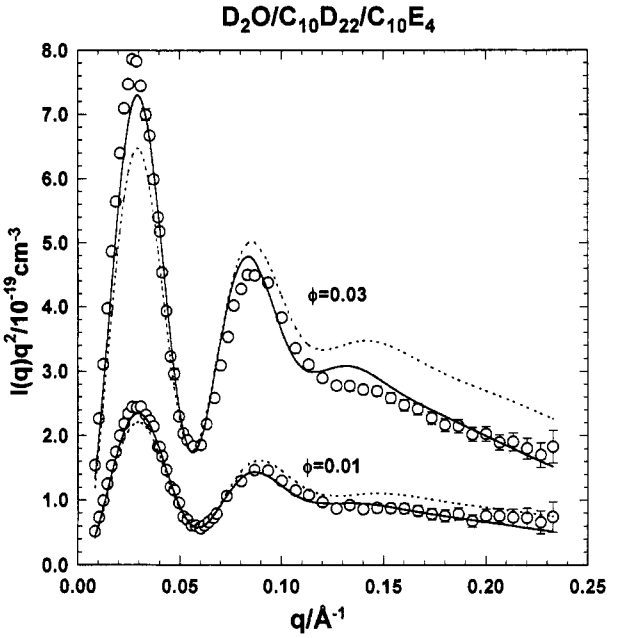

Figure 5. $I(q)q^2$ representation of the SANS intensity for some O/W microemulsions of the $D_2O/C_{10}D_{22}/C_{10}E_4$ system for droplet volume fractions ϕ = 0.01 and 0.03 at T = 10 °C. The microemulsion was always just saturated with oil, i.e., at the phase boundary and in equilibrium with a small amount of excess oil phase. The solid lines are the fits according to eq 11. The dashed lines are calculated with the sharp boundary shell model (eq 13). Note the improved description by the diffuse shell model over the whole q range.

TABLE 1: Mean Radius r_0, Shell Thickness δ or Thickness Parameter t, and Polydispersity Index $p = \sigma/r_0$ (Still Including the Experimental Resolution Function) for the System $D_2O/C_{10}D_{22}/C_{10}E_4$ at 10 °C As Obtained by the New Model (I) and by the Shell Model with Sharp Boundaries (II)

volume fraction	I			II		
	r_0/Å	t/Å	p	r_0/Å	δ/Å	p
0.00997	48.1	4.57	0.194	48.2	12.0	0.193
0.0309	50.6	4.71	0.187	50.5	12.4	0.189

We nevertheless calculated a hard-sphere structure factor[52] for our samples, which, however, differed only insignificantly from unity. The data were taken on PAXE with λ = 6 Å, $\Delta\lambda/\lambda$ = 0.1, data treatment as in ref 28. The details of these experiments will be described in a separate paper.[53]

Since these experiment were aimed at examining the low- and intermediate-q range of the particle form factor for NSE experiments, the background scattering was not recorded and could not be determined directly. Therefore the scattering of the solvent (0.086 cm^{-1}) and the incoherent scattering in proportion to the surfactant volume fraction (0.006 for ϕ = 0.01 and 0.018 for ϕ = 0.03) was subtracted as I_b. Plotting the data, as done in Figure 5, in the form $I(q)q^2$ vs q permits us to recognize the improved description by the diffuse interface approach. It reveals that not only the large-q part is significantly better described but also the intermediate range of the maxima where the conventional model clearly much more over- or undershoots.

The quantitative analysis yields the mean radii r_0, the effective shell thickness (to yield the same total mass of the shell t should be about equal to $\delta/(2\pi)$,[0.5] eq 4), and the polydispersity index $p = \sigma/r_0$ (Table 1). The δ we obtain is in close agreement with that of Lee and Chen.[55] Quite good agreement of the radii for both models is observed. Yet the new model seems to be the more realistic one to describe such microemulsion droplets,

since one may not expect the amphiphile to form very abrupt interfaces. On the contrary, most investigations on micellar and microemulsion systems have shown significant solvent penetration to occur at the hydrophilic/hydrophobic interface. We note that the indirect Fourier transformation technique developed by Glatter[56] directly yields the scattering length distribution if the symmetry is known. Such work is in progress.

IV. Conclusions

The particle form factor, i.e., the angle-dependent scattering intensity resulting from intraparticle interferences, has been derived for shell-structured particles, where the shell has a Gaussian profile of the scattering length density distributed around the shell radius r_0. The model is extended to also include the effect of polydispersity where the distribution of the shell radii is described by a Gaussian distribution, while the thickness of the shell (described by the variance t of the Gaussian density profile) is kept constant. Such a model still yields an analytical solution for the corresponding form factor.

The form factor has then been compared to that of the more conventional model with sharp shell boundaries. Both models yield principally similar scattering patterns, with the exception of high-q range. There, the model with diffuse boundaries predicts an exponentially steep decrease of the intensity with increasing q. It was anticipated that this model might be appropriate for the description of microemulsion droplets because here some penetration of oil into the hydrophobic part and of water into the hydrophilic part of the amphiphilic layer is expected to occur. This effect should be roughly symmetrical for non-ionic surfactants of the alkylpoly(glycol ether) type, C_iE_j, and therefore the Gaussian density profile be a good description of the actual situation.

For the ternary microemulsion systems water/oil/$C_{10}E_4$ SANS data were compared with the predicted scattering intensity. Extending the measurements to sufficiently high q permitted to determine the background scattering directly, and evidence for the steep decay is clearly demonstrated. The present investigation thus confirms the previous experiments on zero-mean curvature structures[42] and extends the conjecture of a diffuseness of internal interfaces in microemulsion to the case of spherical droplets.

It was furthermore found that the experimental data are very well described by three parameters, mean radius r_0, thickness parameter t, and polydispersity index $p = \sigma/r_0$. A comparison with the conventional model with sharp boundaries shows an improved agreement of the new model with the experimental data, particularly in the high-q range.

The model is a suitable tool for the interpretation of experimental scattering data of shell structured microemulsions and vesicles. Despite the fact that it describes a relatively complex situation, i.e., it takes into account the diffuseness of the interfacial region and allows for a polydispersity of the aggregates, the model still provides a simple analytical expression for the particle form factor.

Acknowledgment. Financial support of this work by a grant of the CEC (ERB4050PL920671) is gratefully acknowledged. M.G. would also like to thank for a postdoctoral stipend of the program Human Capital and Mobility (ERB4001GT931413), also financed by the European Union, allowing him to participate in this research.

Appendix

We seek the solution of the normalized integral

$$I(2\pi)^{1/2}\sigma = \int_{-\infty}^{+\infty}(r\sin qr + qt^2\cos qr)^2 \exp\left(-\frac{(r-r_0)^2}{2\sigma^2}\right) dr \quad \text{(A1)}$$

Using the relations $\sin 2x = 2\sin x \cos x$, $\sin^2 x = 1/2\ (1-\cos 2x)$ and $\cos^2 x = 1/2\ (1+\cos 2x)$ and the substitution $r = a + \sigma z$, that is $dr = \sigma dz$, $a = r_0$, $b = 2q$ and $c = qt^2$ one obtains

$$I(2\pi)^{1/2}\sigma = \frac{1}{2}(I_1 + I_2 + I_3) \quad \text{(A2)}$$

$$I_1 = \sigma c^2 \int_{-\infty}^{+\infty}[1 + \cos(ab + \sigma bz)\exp(-z^2/2)]\, dz = \sigma(2\pi)^{1/2}[c^2(1 + \cos ab\, \exp(-\sigma^2 b^2/2))] \quad \text{(A3)}$$

$$I_2 = 2\sigma c \int_{-\infty}^{+\infty}(a + \sigma z)\sin(ab + \sigma bz)\exp(-z^2/2)\, dz = \sigma(2\pi)^{1/2}[2c(a\sin ab + \sigma^2 b\cos ab)\exp(-\sigma^2 b^2/2)] \quad \text{(A4)}$$

$$I_3 = \sigma\int_{-\infty}^{+\infty}(a + \sigma z)^2[1 - \cos(ab + \sigma bz)\exp(-z^2/2)]\, dz = \sigma(2\pi)^{1/2}[a^2 + \sigma^2] - \sigma(2\pi)^{1/2}[a^2\cos ab\, \exp(-\sigma^2 b^2/2)] - \sigma(2\pi)^{1/2}[-2\sigma^2 ab\sin ab\, \exp(-\sigma^2 b^2/2)] - \sigma(2\pi)^{1/2}[\sigma^2\cos ab(1 - \sigma^2 b^2)\exp(-\sigma^2 b^2/2)] \quad \text{(A5)}$$

The normalizing factor drops out, and resubstitution of a, b, and c then yields[51]

$$I(q) = t_1(q) + t_2(q) + t_3(q) + t_4(q) \quad \text{(A6)}$$

$$t_1(q) = {}^1/_2 q^2 t^4(1 + \cos 2qr_0 e^{-2\sigma^2 q^2}) \quad \text{(9a)}$$

$$t_2(q) = qt^2(r_0\sin 2qr_0 + 2q\sigma^2\cos 2qr_0)e^{-2\sigma^2 q^2} \quad \text{(9b)}$$

$$t_3(q) = {}^1/_2 r_0^2(1 - \cos 2qr_0 e^{-2\sigma^2 q^2}) \quad \text{(9c)}$$

$$t_4(q) = {}^1/_2\sigma^2(1 + 4qr_0\sin 2qr_0 e^{-2\sigma^2 q^2} + \cos 2qr_0(4\sigma^2 q^2 - 1)e^{-2\sigma^2 q^2}) \quad \text{(9d)}$$

References and Notes

(1) Prince, L. M. *Microemulsions: Theory and Practice*; Academic Press: New York, 1977.
(2) Langevin, D. *Mol. Cryst. Liq. Cryst.* **1986**, *138*, 259.
(3) Hoar, T. P.; Schulman, J. H. *Nature* **1943**, *152*, 102.
(4) Schulman, J. H.; Stoeckenius, W.; Prince, L. M. *J. Phys. Chem.* **1959**, *63*, 1677.
(5) Winsor, P. A. *Solvent Properties of Amphiphilic Compounds*; Butterworth: Scientific Publications: London, 1954.
(6) Ober, R.; Taupin, C. *J. Phys. Chem.* **1980**, *84*, 2418.
(7) Hoffmann, H.; Platz, G.; Ulbricht, W. *Ber. Bunsenges. Phys. Chem.* **1986**, *90*, 877.
(8) Kotlarchyk, M.; Chen, S. H.; Huang, J. S.; Kim, M. W. *Phys. Rev. A* **1984**, *29*, 2054.
(9) Dvolaitzky, M.; Guyot, M.; Lagues, M.; Le Pesant, J. P.; Ober, R.; Sauterey, C.; Taupin, C. *J. Chem. Phys.* **1978**, *69*, 3279.
(10) Cazabat, A. M.; Langevin, D. *J. Chem. Phys.* **1981**, *74*, 3148.
(11) Graciaa, A.; Lachaise, J.; Chabrat, P.; Letamendia, L.; Rouch, J.; Vaucamps, C. *J. Phys. Lett. (Paris)* **1978**, *39*, L-235.
(12) Scriven, L. E. *Nature* **1976**, *263*, 123.
(13) Auvray, L.; Cotton, J. P.; Ober, R.; Taupin, C. *Physica* **1986**, *136B*, 281.
(14) Ceglie, A.; Das, K. P.; Lindman, B. *Colloids Surf.* **1987**, *28*, 29.
(15) Kaler, E. W.; Bennett, K. E.; Davis, H. T.; Scriven, L. E. *J. Chem. Phys.* **1983**, *79*, 5673.
(16) Talmon, Y.; Prager, S. *J. Chem. Phys.* **1982**, *76*, 1535.
(17) de Gennes, P. G.; Taupin, C. *J. Phys. Chem.* **1982**, *86*, 2294.

(18) Zemb, T. N.; Barnes, I. S.; Derian, P. J.; Ninham, B. W. *Prog. Colloid Polym. Sci.* **1990**, *81*, 20.
(19) Chen, S. H.; Chang, S. L.; Strey, R. *Prog. Colloid Polym. Sci.* **1990**, *81*, 30.
(20) Barnes, I. S.; Hyde, S. T.; Ninham, B. W.; Derian, P. J.; Drifford, M.; Zemb, T. N. *J. Phys. Chem.* **1988**, 92, 2286.
(21) Ben Azouz, I.; Ober, R.; Nakache, E.; Williams, C. E. *Colloids Surf.* **1992**, *69*, 87.
(22) Cazabat, A. M.; Langevin, D.; Pouchelon, A. *J. Colloid Interface Sci.* **1980**, *73*, 1.
(23) Cabane, B.; Duplessix, R.; Zemb, T. *J. Physique* **1985**, *46*, 2161.
(24) Kotlarchyk, M. *Physica* **1986**, *136B*, 274.
(25) Chang, N. J.; Kaler, E. *Langmuir* **1986**, *2*, 184.
(26) Huang, J. S.; Sung, J.; Wu, X.-L. *J. Colloid Interface Sci.* **1989**, *132*, 34.
(27) Chou, S. I.; Shah, D. O. *J. Colloid Interface Sci.* **1981**, *80*, 49.
(28) Sicoli, F.; Langevin, D.; Lee, L. T. *J. Chem. Phys.* **1993**, *99*, 4759.
(29) Huang, J. S.; Sung, J.; Wu, X.-L. *J. Colloid Interface Sci.* **1989**, *132*, 34.
(30) Strey, R. *Colloid Polym. Sci.* **1994**, *272*, 1005.
(31) Caponetti, E.; Magid, L. J. In Microemulsion Systems. *Surf. Sci. Ser.* Rosano, H. L., Clausse, M., Eds.; Marcel Dekker Inc.: New York, Basel, 1987; Vol. 24, p 299.
(32) Markovic, I.; Ottewill, R. H. *Colloid Polym. Sci.* **1986**, *264*, 65.
(33) Ottewill, R. H.; Sinagra, E.; Mac Donald, I. P.; Marsh, J. F.; Heenan, R. K. *Colloid Polym. Sci.* **1992**, *270*, 602.
(34) Moonen, J. A. H. M.; de Kruif, C. G.; Vrij, A.; Bantle, S. *Colloid Polym. Sci.* **1988**, *266*, 836.
(35) Cabos, C.; Delord, P.; Martin, J. C. *J. Phys.* **1979**, *40*, 407.
(36) Tabony, J. *Mol. Phys.* **1984**, *51*, 975.
(37) Hayter, J. B.; Penfold, J. P. *J. Chem. Soc., Faraday Trans. I* **1981**, *77*, 1851.
(38) Triolo, R.; Hayter, J. B.; Magid, L. J.; Johnson, J. S. Jr. *J. Chem. Phys.* **1983**, *79*, 1977.
(39) Zemb, T.; Charpin, P. *J. Phys.* **1985**, *46*, 249.
(40) Skov Pedersen, J. *Eur. Biophys. J.* **1993**, *22*, 79.
(41) Bauer, R.; Behan, M.; Clark, D.; Hansen, S.; Jones, G.; Mortensen, K.; Skov Pedersen, J. *Eur. Biophys. J.* **1992**, *21*, 129.
(42) Strey, R.; Winkler, J.; Magid, L. *J. Phys. Chem.* **1991**, *95*, 7502.
(43) Cebula, D. J.; Ottewill, R. H.; Ralston, J.; Pusey, P. N. *J. Chem. Soc., Faraday Trans. 1* **1981**, *77*, 2585.
(44) Aragon, S. R.; Pecora, R. *J. Chem. Phys.* **1976**, *64*, 2395.
(45) Ruland, W. *J. Appl. Cryst.* **1971**, *4*, 70.
(46) Saito, H.; Shinoda, K. *J. Colloid Interface Sci.* **1967**, *24*, 10.
(47) Shinoda, K.; Friberg, S. *Adv. Colloid Interface Sci.* **1975**, *4*, 281.
(48) Kahlweit, M.; Strey, R. *Angew. Chem. Int. Ed. Engl.* **1985**, *24*, 654.
(49) Olsson, U.; Nagai, K.; Wennerström, H. *J. Phys. Chem.* **1988**, *92*, 6675.
(50) Magid, L.; Butler, P.; Payne, K.; Strey, R. *J. Appl. Cryst.* **1988**, *21*, 832.
(51) Note that in ref. 30 part of the t_4 term is missing. The omission leads to a change of the obtained radii of the order of 3−5%, which is, however, still within the symbol width of Figures 10 and 11 in ref. 30.
(52) Ashcroft, N. W.; Lekner, J. *Phys. Rev.* **1966**, *145*, 83.
(53) Farago, B.; Gradzielski, M.; Langevin, D. To be published.
(54) Billman J. F.; Kaler, E. W. *Langmuir* **1991**, *7*, 1609.
(55) Lee, D. D.; Chen, S. H. *Phys. Rev. Lett.* **1994**, *73*, 106.
(56) Glatter, O. *Prog. Colloid Polym. Sci.* **1991**, *84*, 46.

JP950782W